**Electronic Supplementary Information:**

# Electrocatalytic Oxidation of 5-Hydroxymethylfurfural to 2,5-Furandicarboxylic Acid on Supported Au and Pd Bimetallic Nanoparticles

David J. Chadderdon[a], Le Xin[a], Ji Qi[a], Yang Qiu[a], Phani Krishna[a], Karren L. More[b], and Wenzhen Li[*a]

a Chemical Engineering Department Michigan Technological University 1400 Townsend Drive, Houghton, MI 49931 (USA) E-mail: wzli@mtu.edu

b Material Science and Technology Division Oak Ridge National Laboratory Oak Ridge, Tennessee 37831 (USA)

Electronic Supplementary Information Contents:

## 1. X-Ray Diffraction (XRD):

XRD patterns for all catalysts were collected from 15° to 90° and displayed a typical face-centered cubic (FCC) pattern with diffraction peaks at ~39°, 46°, 67°, and 80° assigned to the corresponding (111), (200), (220), and (311) facets, respectively as seen in Fig. S1. There is a clear shift in peak position with changing metal composition, implying that alloyed crystal structures are present in $Pd_2Au_1/C$ and $Pd_1Au_2/C$. Average crystal size was calculated from the (220) diffraction peak with the Debye-Scherrer formula (Eqn. S1)

$$L = 0.9\lambda_{K\alpha} / \beta_{2\theta}\cos(\theta_{max}) \qquad\qquad (S1)$$

where L is the average crystal size, $\lambda_{K\alpha}$ is the X-ray wavelength (1.5406 Å), $\beta_{2\theta}$ is the full width at half height of the (220) peak in radians, and $\theta_{max}$ is the Bragg angle in radians. The calculated average crystal sizes are summarized in main text (Table 1), and found to be consistent with the TEM particle size histograms.
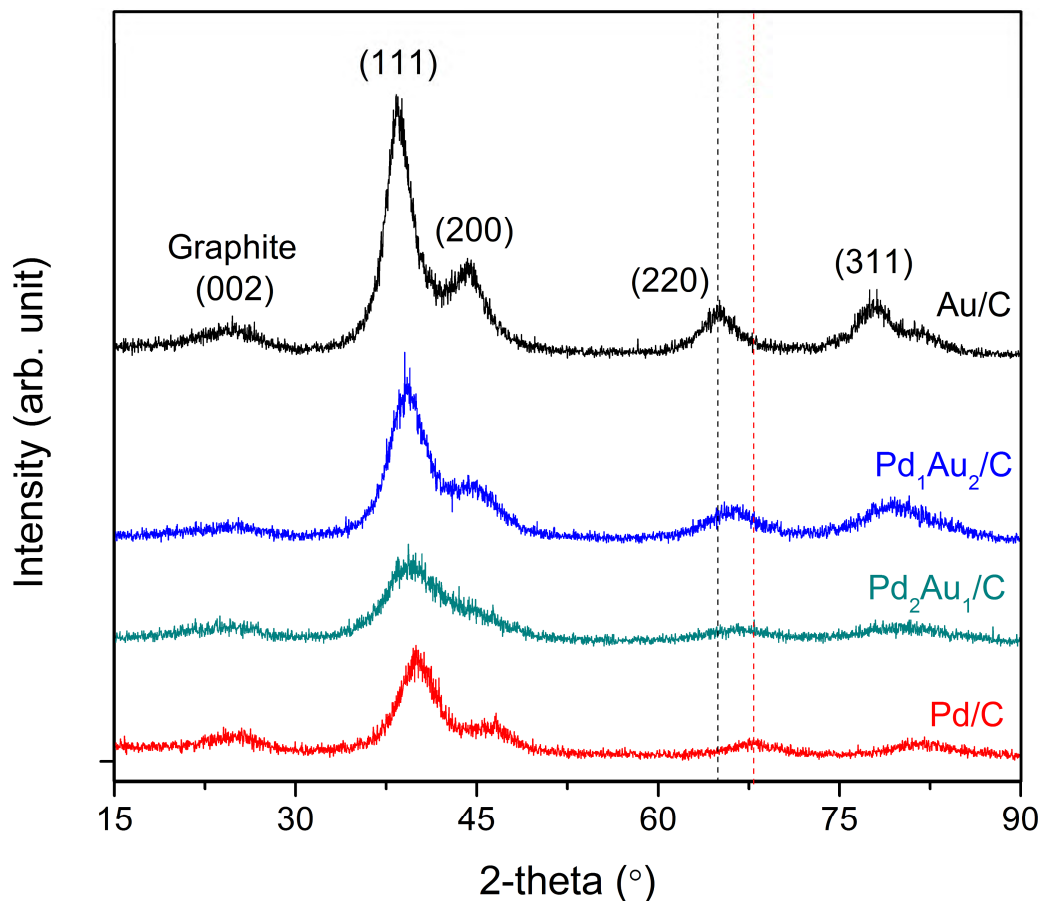


**Fig. S1** XRD patterns of self-prepared Pd/C, $Pd_2Au_1/C$, $Pd_1Au_2/C$, and Au/C catalysts. Peak position shift is observed as metal composition varies, indicating that alloyed crystal structures are present in the $Pd_2Au_1/C$ and $Pd_1Au_2/C$ samples. The peaks for $Pd_2Au_1/C$ and $Pd_1Au_2/C$ are in between Pd/C and Au/C, as noted with vertical dashed lines for the (220) peak.

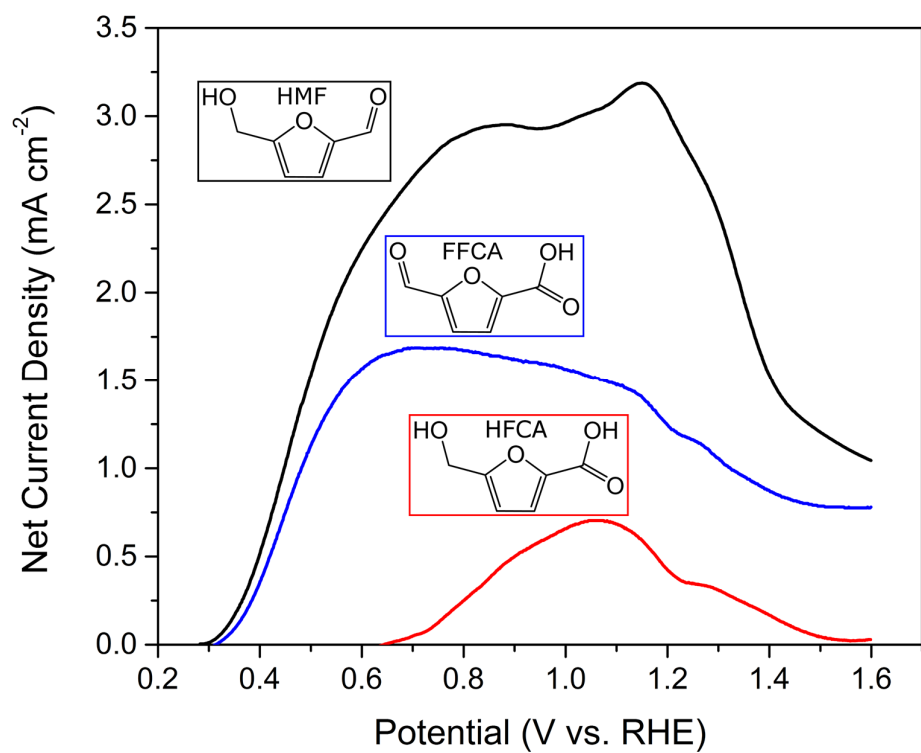## 2. Cyclic voltammetry of HMF, HFCA, and FFCA on Au/C and Pd/C



**Fig. S2** Anodic-scan from half-cell cyclic voltammetry of 0.1 M KOH with 0.02 M HMF, HFCA, and FFCA on Au/C. Net current density is difference of anodic-scan current density and blank current density (0.1 M KOH only test). Reaction conditions: 50 mL solution; 25 °C; scan rate 50 mV sec$^{-1}$.

**Fig. S3** Anodic-scan from half-cell cyclic voltammetry of 0.1 M KOH with 0.02 M HMF, HFCA, and FFCA on Pd/C. Net current density is difference of anodic-scan current density and blank current density (0.1 M KOH only test). Reaction conditions: 50 mL solution; 25 °C; scan rate 50 mV sec$^{-1}$.
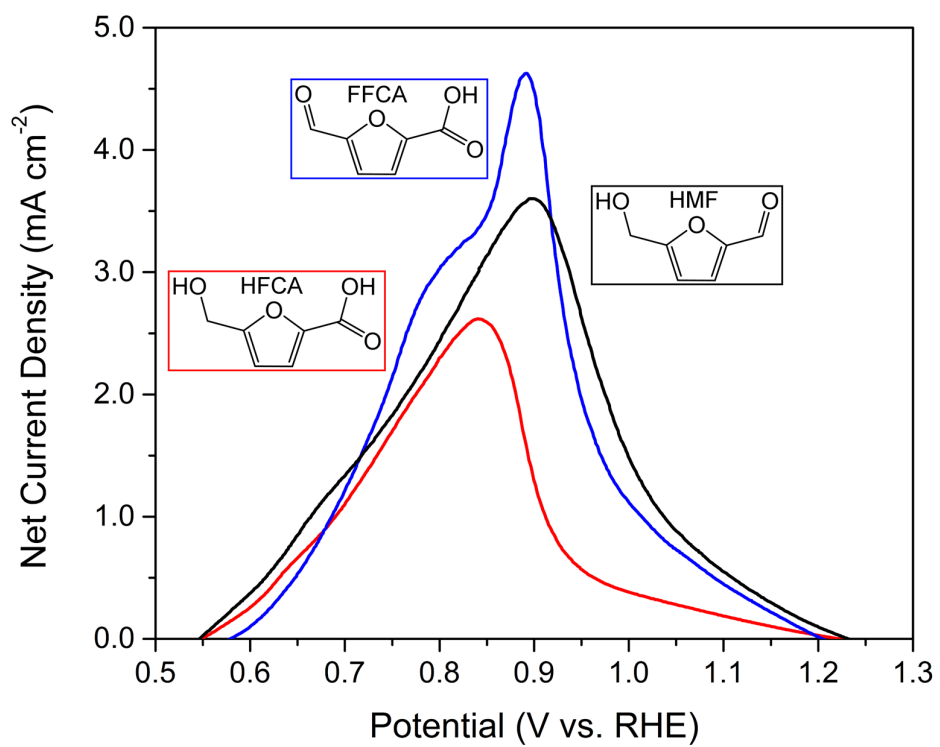
## 3. Cyclic voltammetry of glyoxylic acid on Pd/C and Au/C:

It was found that oxidation of the aldehyde group of HMF or FFCA (See Fig. 4A,C) proceeded on Au/C at much lower potentials than Pd/C. Analogously, cyclic voltammetry was performed under identical conditions as Fig. 4 except with glyoxylic acid in solution, and the results are shown in Fig. S4. Oxidation onset potential shifted about 140 mV more negative on Au/C than Pd/C for glyoxalylic oxidation, compared to about 260 mV shift observed for HMF and FFCA. The difference may be attributed to even more difficult oxidation on Pd/C when the aldehyde is attached to the furan-ring structure found in HMF and FFCA.
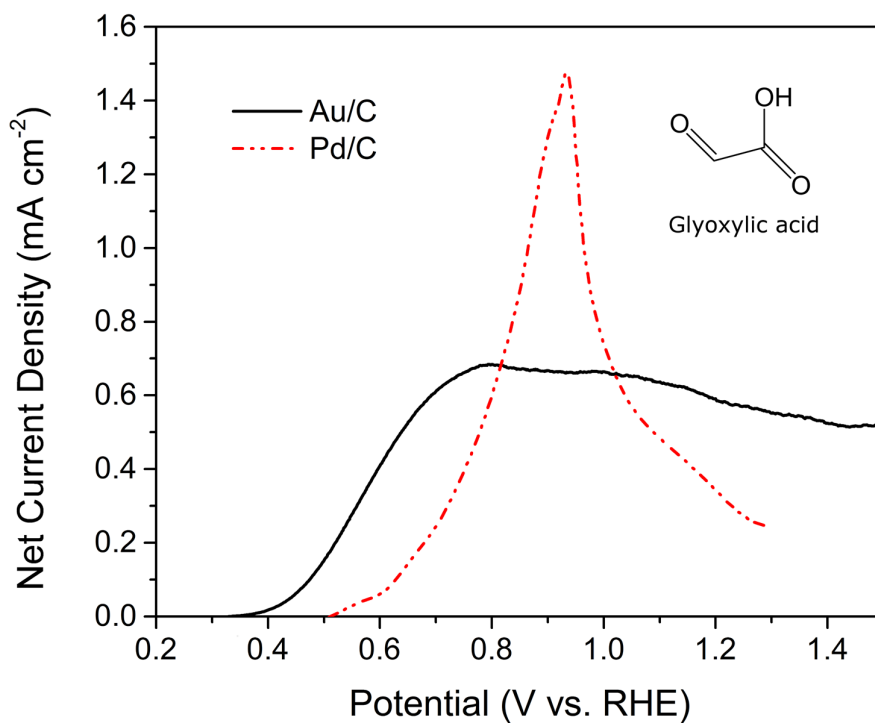


**Fig. S4** Anodic-scan from half-cell cyclic voltammetry of 0.1 M KOH with 0.02 M glyoxylic acid. Net current density is difference of anodic-scan current density and blank current density (0.1 M KOH only test). Reaction conditions: 50 mL solution; 25 °C; scan rate 50 mV sec$^{-1}$.

## 4. Reaction product profiles for AEM-electrolysis flow reactor on Pd$_2$Au$_1$/C and Pd$_1$Au$_2$/C electrocatalysts:

Time-dependent product distribution can reveal further insight into the effect of catalyst on reaction mechanism and pathway. Time-dependent HMF conversion and product selectivity for 2 h reaction at 0.6V vs. RHE on alloyed Pd$_2$Au$_1$/C and Pd$_1$Au$_2$/C catalysts are shown in Fig. S5 (Results on Pd/C and Au/C are shown in main text, Fig. 5). Fig. S5, clearly demonstrates the advantages of increased Au-content in alloyed catalysts for FDCA formation. The Pd-rich alloy behaved very similarly to pure Pd/C at 0.6 V, with FFCA as the main observed product and notable amounts of FDA detected at shorter reaction times. The Au-rich catalyst has greatly enhanced aldehyde group oxidation, evidenced by large amount of HFCA (resulting from HMF aldehyde group oxidation), the absence of di-aldehyde FDA, and increased selectivity to the di-acid FDCA.
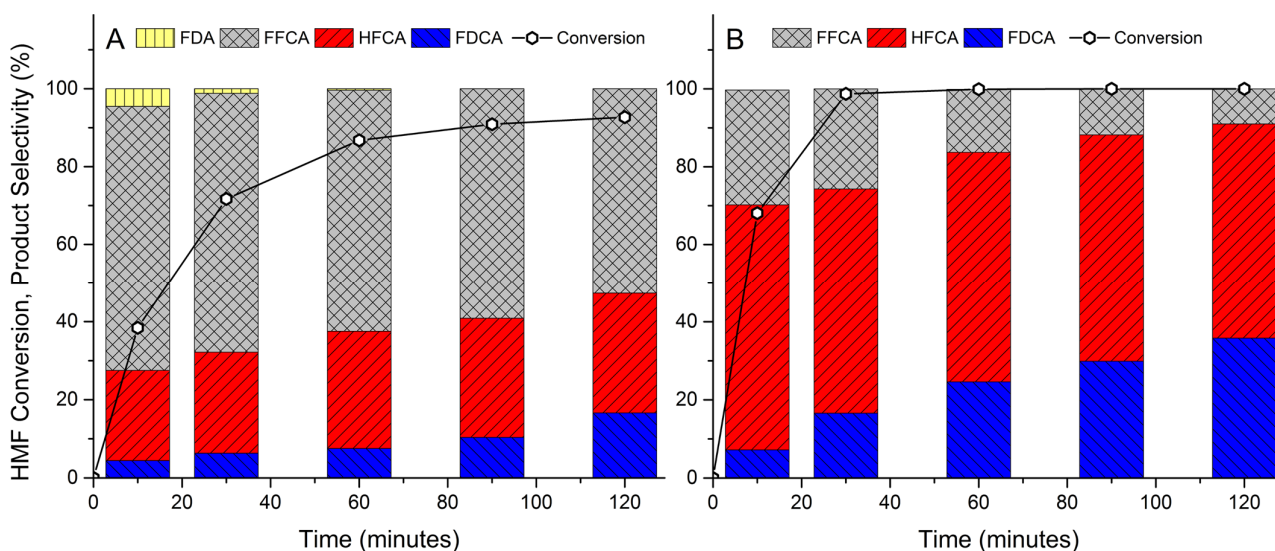


**Fig. S5** Reaction product profiles for oxidation of HMF over (A) Pd$_2$Au$_1$/C and (B) Pd$_1$Au$_2$/C including HMF conversion and product selectivity. Reaction conditions: 25 mL of 0.02 M HMF + 0.1 M KOH solution; flow 20 mL min$^{-1}$; 25 °C; anode potential 0.6 V vs. RHE.

## 5. Cannizzaro's reaction:

HMF, FDA, and FFCA contain aldehyde-groups and may undergo the Cannizzaro reaction in alkaline conditions. In bulk alkaline solution, intramolecular reduction/oxidation may result in the following reactions:

$$2\ HMF \rightarrow DHMF + HFCA$$
$$2\ FDA \rightarrow HMF + FFCA$$
$$2\ FFCA \rightarrow HFCA + FDCA$$
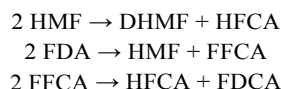
where DHMF is 2,5-dihydroxymethylfurfural. It is hypothesized that these reactions will be negligible compared to the rate of electrocatalytic oxidation under these conditions of mild alkaline conditions (0.1 M KOH, pH 13) and low species concentration (0.02 M maximum). Since FDA is key intermediate for identifying reaction pathway, a control test of 0.02 M FDA in 0.1 M KOH was performed in the absence of catalyst or applied potential. The test confirmed that the Cannizzaro's reaction is quite slow under these conditions, with less than 10% of FDA converted to equimolar HMF and FFCA after 1 h reaction.

## 6. Estimation of alloy surface composition by cyclic voltammetry

The nature and surface atomic compositions of Pd-Au alloys were determined by electrochemical methods proposed by Rand and Woods.[43] In cyclic voltammetry (CV), the metal-oxide reduction peak position depends on catalyst surface composition, and this dependence was found by Rand and Woods to be linear for the Pd-Au system. In other words, the composition of alloyed phases on the catalyst surface can be estimated by the degree of peak shift. Therefore, CV tests can reveal the presence of pure Pd and Au phases, as well as estimate the composition of any alloyed phases. The linear dependence of metal-oxide reduction peak position ($\varphi$) on alloy surface composition ($x_{Pd}$, $x_{Au}$ in at%) is shown by Eqn. S2.

$$\varphi_{alloy} = x_{Pd}\ \varphi_{Pd} + x_{Au}\ \varphi_{Au} \tag{S2}$$

CV was performed in 0.1 M KOH electrolyte to determine the metal-oxide reduction peak positions and the resulting curves for alloyed catalysts and pure Pd/C and Au/C are shown in Fig. 6 in the main text. The metal-oxide reduction peak location and estimated surface fractions are shown in Table S1, as well as a comparison to the bulk metal composition measurements by ICP-AES and STEM-EDS. Note that two reduction peaks were observed for $Pd_1Au_2$/C which is evidence of two metal phases present at the surface, Pd-Au alloyed and pure Au phases. Whereas, only one reduction peak was observed for $Pd_2Au_1$/C, suggesting only a single alloyed phase was present at the catalyst surface and no monometallic phases were present.

**Table S1.** Metal-oxide reduction peak location and estimated surface composition [a]

| Catalyst | Reduction peak potential, $\varphi$ [V vs. RHE] | Pd surface fraction, $x_{Pd}$ [at%] | Pd bulk fraction [b] [at%] | Pd bulk fraction [c] [at%] |
|---|---|---|---|---|
| Pd/C | 0.57 | - | - | - |
| $Pd_2Au_1$/C | 0.70 | 72 | 64 | 63 |
| $Pd_1Au_2$/C [d] | 0.79 | 53 | 36 | 30 |
| | 1.06 | - | - | - |
| Au/C | 1.04 | - | - | - |

[a] Reaction conditions: CV with 50 mL of 0.1 M KOH electrolyte; 25 °C; 20 μg catalyst loading on glassy-carbon electrode; scan rate 50 mV sec$^{-1}$.

[b] From ICP-AES

[c] From STEM-EDS

[d] Two reduction peaks present for $Pd_1Au_2$/C